



HAL
open science

Water transparency measurements in the deep Ionian Sea

E.G. Anassontzis, A.E. Ball, A. Belias, A. Fotiou, G. Grammatikakis, H. Kontogiannis, P. Koske, S. Koutsoukos, V. Lykoussis, E. Markopoulos, et al.

► **To cite this version:**

E.G. Anassontzis, A.E. Ball, A. Belias, A. Fotiou, G. Grammatikakis, et al.. Water transparency measurements in the deep Ionian Sea. *Astroparticle Physics*, 2010, 34 (4), pp.187. 10.1016/j.astropartphys.2010.06.008 . hal-00679742

HAL Id: hal-00679742

<https://hal.science/hal-00679742>

Submitted on 16 Mar 2012

HAL is a multi-disciplinary open access archive for the deposit and dissemination of scientific research documents, whether they are published or not. The documents may come from teaching and research institutions in France or abroad, or from public or private research centers.

L'archive ouverte pluridisciplinaire **HAL**, est destinée au dépôt et à la diffusion de documents scientifiques de niveau recherche, publiés ou non, émanant des établissements d'enseignement et de recherche français ou étrangers, des laboratoires publics ou privés.

Accepted Manuscript

Water transparency measurements in the deep Ionian Sea

E.G. Anassontzis, A.E. Ball, A. Belias, A. Fotiou, G. Grammatikakis, H. Kontogiannis, P. Koske, S. Koutsoukos, V. Lykoussis, E. Markopoulos, A. Psallidas, L.K. Resvanis, I. Siotis, S. Stavrakakis, G. Stavropoulos, V.A. Zhukov

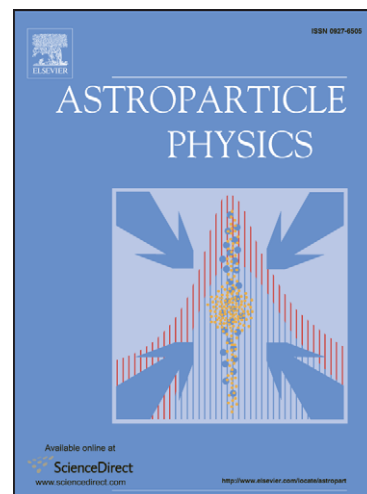
PII: S0927-6505(10)00120-9
DOI: [10.1016/j.astropartphys.2010.06.008](https://doi.org/10.1016/j.astropartphys.2010.06.008)
Reference: ASTPHY 1504

To appear in: *Astroparticle Physics*

Received Date: 1 April 2010
Revised Date: 26 June 2010
Accepted Date: 27 June 2010

Please cite this article as: E.G. Anassontzis, A.E. Ball, A. Belias, A. Fotiou, G. Grammatikakis, H. Kontogiannis, P. Koske, S. Koutsoukos, V. Lykoussis, E. Markopoulos, A. Psallidas, L.K. Resvanis, I. Siotis, S. Stavrakakis, G. Stavropoulos, V.A. Zhukov, Water transparency measurements in the deep Ionian Sea, *Astroparticle Physics* (2010), doi: [10.1016/j.astropartphys.2010.06.008](https://doi.org/10.1016/j.astropartphys.2010.06.008)

This is a PDF file of an unedited manuscript that has been accepted for publication. As a service to our customers we are providing this early version of the manuscript. The manuscript will undergo copyediting, typesetting, and review of the resulting proof before it is published in its final form. Please note that during the production process errors may be discovered which could affect the content, and all legal disclaimers that apply to the journal pertain.



1 **WATER TRANSPARENCY MEASUREMENTS IN THE DEEP IONIAN SEA**

2 E.G. Anassontzis^{a,*}, A.E. Ball^{b,c}, A. Belias^c, A. Fotiou^c, G.Grammatikakis^d, H. Kontogiannis^e,
 3 P. Koske^f, S. Koutsoukos^c, V. Lykoussis^e, E. Markopoulos^c, A. Psallidas^c, L.K.Resvanis^{a,c},
 4 I. Siotis^g, S. Stavrakakis^e, G. Stavropoulos^c, V.A. Zhukov^{h,i}

5 ^a *Physics Department, University of Athens, Athens, Greece*

6 ^b *Formerly of CERN (European Organization for Nuclear Research), Geneva, Switzerland*

7 ^c *NESTOR Institute for Deep Sea Research, Technology and Neutrino Astroparticle Physics,*

8 *National Observatory of Athens, Pylos, Greece*

9 ^d *Physics Department, University of Crete, Greece*

10 ^e *Institute of Oceanography, Hellenic Center for Marine Research, Anavyssos, Greece*

11 ^f *Institute of Experimental and Applied Physics, University of Kiel, Kiel, Germany*

12 ^g *Institute of Nuclear Physics, National Center for Scientific Research 'Demokritos', Athens, Greece*

13 ^h *Institute For Nuclear Research, Russian Academy of Sciences, Moscow, Russia, and*

14 ⁱ *Moscow State Open University, Moscow, Russia*

15

16 **Abstract**

17 A long optical base line spectrophotometer designed to measure light transmission in deep sea
 18 waters is described. The variable optical path length allows measurements without the need for
 19 absolute or external calibration. The spectrophotometer uses eight groups of uncollimated light
 20 sources emitting in the range 370 nm-530 nm and was deployed at various depths at two locations
 21 in the Ionian Sea that are candidate sites for a future underwater neutrino telescope. Light
 22 transmission spectra at the two locations are presented and compared.
 23

24 **1. Introduction**

25 The study of high energy neutrinos of astrophysical origin requires the use of very large target
 26 masses, in order to observe a reasonable number of neutrino interactions given the small
 27 interaction cross section for neutrino-nucleon scattering. The observation, mainly via the
 28 production of muons, relies on the detection of the Cherenkov radiation produced and thus
 29 requires an optically transparent target material. Such large amounts of target material can be
 30 most easily obtained by using naturally abundant and transparent media, such as water or ice.
 31 Currently the world's largest neutrino telescope, IceCube[1], is nearing completion at the South
 32 Pole and will encompass one cubic kilometre of glacial ice in its final configuration. In contrast,
 33 the proposed KM3NeT detector (Kilometer cube Neutrino Telescope) [2], a neutrino telescope
 34 planned to be a few times larger than IceCube, will be deployed in the Mediterranean Sea and
 35 thus will use sea water as its detection medium.

* Corresponding author, e-mail: eanason@phys.uoa.gr

Assis. Prof. E. G. Anassontzis
N. & K. UNIVERSITY OF ATHENS
FACULTY of PHYSICS
Nuclear and Particle Physics Department
Panepistimioupolis, Ilissia
GR – 15771 - Athens
 Tel&fax: (+30) 210 7276948

1 In charged current interactions of muon-neutrinos with sea water or underlying rock, the
2 produced high-energy muons travel faster than the speed of light in water and thus emit
3 Cherenkov light that provides the primary observation mode of such a detector. Muons lose very
4 little energy as they travel through matter, and thus have a very long range (e.g. ≈ 7.8 km for
5 $E_{\mu}=10\text{TeV}$). They can therefore be produced far from the detector and still be observed. As a
6 result the effective interaction target volume is equal to the cross sectional area of the detector
7 multiplied by the muon range.

8 The detector itself will consist of a three dimensional lattice of photomultipliers that detect the
9 Cherenkov light and record the time of its arrival and its amplitude. This information is used to
10 reconstruct the direction of the muon, to obtain a rough estimate of its energy and thus to extract a
11 measure of the parent neutrino direction and energy. The photomultipliers are contained in glass
12 spheres capable of withstanding high pressure. These so called “optical modules” (OM) are
13 deployed at great depth where there is no ambient light.

14 Upwards moving and near horizontal muons arising from neutrino interactions in the surrounding
15 earth or water are one of the primary signals in such a neutrino telescope. For neutrinos arriving
16 from below the horizon, the earth serves as a shield against cosmic ray-induced muons. For very
17 high energy neutrinos (>50 TeV), the earth also attenuates the neutrino flux, and for energies
18 above 500 TeV it is essentially opaque. For a neutrino telescope deployed at a large depth (> 4
19 kmwe) the surrounding water attenuates the downwards moving (background) cosmic ray-
20 induced muons, and provides an enhanced solid angle for very high energy neutrinos thus
21 allowing the detection of neutrinos coming from small zenith angles (i.e. coming from directly
22 above) and all the way down to the horizon. This shift from neutrino sensitivity for upwards
23 moving neutrinos at lower energies to downwards moving neutrinos at higher energy is
24 accompanied by a flux reduction which is somewhat compensated by the increasing neutrino
25 cross-section. This however only applies to detectors sufficiently deep to take advantage of the
26 cosmic ray shielding provided by a large overburden.

27 The spacing between the optical modules is determined by the transparency of the sea water.
28 Greater water transparency allows for a sparser detector, leading to a larger detector mass and
29 cross sectional area for the same number of deployed optical modules. As a result, the selection of
30 a deployment site with the clearest waters is of paramount importance in the construction of a
31 large underwater neutrino telescope if one wants to maximize the detector’s sensitivity for given
32 resources. Since the spacing between optical modules will scale with some characteristic water
33 transparency length, *a fortiori*, the effective volume of a detector, for a fixed number of optical
34 modules, will depend on the water transparency. The exact scaling of such detector properties
35 will have to be determined by detailed Monte-Carlo simulation studies. Optical scattering of the
36 Cherenkov radiation affects the angular resolution of such telescopes. In sum, the energy and
37 angular resolution of the detector depends on the optical properties of the water and a precise
38 knowledge of them is required for a proper interpretation of the experimental data.

39 In the Ionian Sea, two candidate areas are under investigation for deploying the KM3NeT: the
40 Pylos area, with a series of plateaus at depths of 3000, 3750, 4550, and 5200 m, located at
41 distances of 13 to 48 km from shore, SW of the city of Pylos, Greece and the Capo Passero area,
42 with depth of 3600 m, located at a distance of 77 to 102 km from shore, SE of Capo Passero, the
43 most south-eastern cape of Sicily, Italy. The Pylos area is where the NESTOR collaboration [3]
44 has operated until now and where a section of the NESTOR neutrino telescope tower has been
45 deployed. The Capo Passero area is where the NEMO collaboration [4] has been active. We have
46 taken measurements of the water clarity at four different sites, two within the Pylos area (N4.5D

1 and N5.2D) and two within the Capo Passero area (CP1 and CP2) and on three different
 2 campaigns; the dates, coordinates and depths of these sites/measurements are shown in Table I.
 3 The deployment campaigns were conducted by the Research Vessel “Aegaeo” of the Hellenic
 4 Centre for Marine Research.

Table I
Dates, locations and depths of measurements

	Site N4.5D			Site N5.2D	Site CP1	Site CP2
Date(s)	April 19-22, 2008	October 23-24, 25-26, 2008	May 9- 10, 2009	October 24-25, 2008	May 6, 2009	May 7, 2009
Coordinates	36°31'N, 21°26'E			36°33'N, 21°08'E	36°11'N, 16°06'E	36°12'N, 15°46'E
Nominal sea depth (m)	4460			5200	3360	3600
Data taking station depth (m)	-	-	-	4900	-	-
	4100	4100	4100	4000	-	-
	3400	3400	3400	-	-	3400
	-	-	3000	3000	3100	3000
	2500	2500	2500	-	2500	2500
	-	2000	2000	2000	2000	2000

5

6 2. Experimental methodology and apparatus

7 The inherent optical properties (IOP) generally chosen by the oceanographic community to
 8 describe the propagation of light in water are:

- 9 • the absorption coefficient $a(\lambda)$ (or the absorption length $L_a = 1/a$)
- 10 • the scattering coefficient $b(\lambda)$ (or the scattering length $L_b = 1/b$)
- 11 • the attenuation coefficient $c = a + b$ (or the attenuation length
 12 $L_c = 1/c = (1/L_a + 1/L_b)^{-1}$)
- 13 • the phase scattering function $\chi(\theta, \lambda)$ (also referred to as the volume scattering
 14 function)

15 We note that the IOPs as measured by the oceanographic community do not optimally address the
 16 needs of a neutrino telescope. The oceanographers use a well-collimated beam where rays
 17 scattered by more than a few mrad are lost, and the attenuation measured is due to the sum of
 18 absorption plus scattering. In the case of a large underwater neutrino telescope, such as the
 19 KM3NeT, to be deployed in extremely clear and clean sea water, the main light attenuation
 20 mechanism is just the absorption since the scattering length is much longer than the absorption
 21 length [5]. Underwater neutrino telescopes operate, using uncollimated Cherenkov photons, in an
 22 “open geometry” regime, because their optical modules have a large angle of photon acceptance.
 23 In such an open geometry experiment, the optical modules will detect the majority of the

1 Cherenkov photons that are initially generated in the direction toward the module plus some of
 2 the scattered photons provided that either of these are not absorbed. Following Bradner *et al.* [6]
 3 we opted to use an open geometry transmissivity meter to measure propagation of light in the sea
 4 water. We use the term transmission length L_β ($\beta = 1/L_\beta$ is then the 1/e transmission coefficient) in
 5 order to avoid confusion with the attenuation length, usually used in experiments with a well-
 6 collimated beam. For the series of measurements reported here we have designed and constructed
 7 an instrument with “open geometry”, and with an optical path appropriate for transparency
 8 measurements in clear waters. We refer to it as the Long Arm Marine Spectrophotometer (the
 9 LAMS) and we have used it to make transparency measurements in the deep Ionian Sea.

10 When the scattering length is much longer than both the absorption length and the measurement
 11 distance R , as it is in our case, the transmission coefficient β can be determined experimentally
 12 from a combined $1/R^2$ and the Beer-Lambert law [7]:

$$13 \quad I(\lambda, R) = \frac{I_0(\lambda)}{4 \cdot \pi \cdot R^2} \cdot e^{-\frac{R}{L_\beta(\lambda)}} \quad (1)$$

14 where $L_\beta = 1/\beta$ is the transmission length and β the transmission coefficient, $I(\lambda, R)$ is the
 15 measured intensity of light of wavelength λ at a distance R from an isotropic light source, and I_0
 16 the intensity of the light source. The relative error in the measurement of β is inversely
 17 proportional to the product $\beta \cdot R$:

$$18 \quad \frac{\Delta\beta}{\beta} = \frac{1}{\beta \cdot R} \cdot \frac{\Delta I}{I} \quad (2)$$

19 We see that in measurement situations where a small value of $\beta \cdot R$ is used, one may have a large
 20 error value even if the light intensity is measured with good accuracy. Therefore, to accurately
 21 measure the transmission coefficient β in clear natural waters, where it has small values, we need
 22 either an instrument with extreme accuracy in measuring light intensity, or an instrument with a
 23 long optical path.

24 The waters at the sites studied show high transparency [5,7] and the correct measurement of the
 25 transmission length is not a simple problem. Commercially available instruments are not well
 26 suited for measurements in very clear water; the small length optical base of such instruments
 27 (usually no more than 1 meter) dictates an increased accuracy of the light intensity measurement.

28 The LAMS, being an open geometry light measuring system, registers not only direct photons
 29 from a light source but also a fraction of the photons scattered in the surrounding water, however
 30 note that it does not register those scattered out of the solid angle defined by the point of origin
 31 and the detector. The scattering length in clear natural water reaches values of more than 200 m
 32 [8]. Since the light path of the LAMS is always much shorter than the scattering length, single
 33 scattering of light propagation dominates.

34

1 2.1 Long Arm Marine Spectrophotometer (LAMS) – Description

2 We studied the water transparency in an open geometry setup, where an uncollimated light beam
 3 was used and where the transmission length was measured. We employed a set of fixed lengths of
 4 optical paths and a simple robust method of measuring the light intensity of LED sources, of
 5 different wavelengths, at these fixed lengths. The technique employed does not need any external
 6 calibration. Moreover, the LAMS design has no movable elements. A rough sketch and a
 7 photograph of the LAMS are shown in Fig.1.

8 The mechanical frame defining the optical path length consists of 5 girders attached to each other
 9 to form a long linear structure; four girders each being 5m long and constructed from titanium
 10 tubing and one girder 2m long made from stainless steel tubing. Special attention was paid to
 11 alignment issues during construction; the girders were built and welded with the aid of a specially
 12 built cradle that allowed for good alignment of the whole structure. The cross-section of the
 13 girders is 40 cm × 40 cm. By adding or removing the appropriate girders the overall frame length
 14 of the instrument could be varied; during our studies we used the lengths of 10.00, 15.10, 17.17,
 15 and 22.27 m for the optical path.

16 The light source and the light detector are each placed in separate 43.2 cm outer diameter glass
 17 spheres [9] (with wall thickness of 1.5 cm) that are fixed on the opposite ends of the frame. In
 18 order to minimise unwanted light reflections, the frame, as well as all glass housing parts that are
 19 not in the light path, are painted with black matte paint. During deployment the frame was
 20 vertical with the light source at the lower end. An additional weight was attached below the frame
 21 in order to provide further vertical stability. Alignment stability is assured by the rigid girder
 22 structure. Initially, the light source and the light detector were attached at the end of two 5m long
 23 girders and were aligned in the laboratory using a laser beam. The light source and the light
 24 detector were mounted on specially constructed frames inside the respective glass spheres and
 25 remained fixed throughout the deployments. This was checked by taking calibration
 26 measurements before and after deployment for all optical path lengths. The distance between the
 27 light source and the detector, as already described, was controlled by adding in-between
 28 appropriate girders.

Table II:

Light source LED parameters (used in Oct 2008 and May 2009 deployments). In April 2008 a different LED matrix was used, however the LEDs consisted of the same types, but taken from different manufacturing batches.

Peak intensity wavelength λ_m (nm)	375.7	385.7	400.3	425.0	445.4	462.6	501.6	519.5
FWHM (nm)	12.9	13.7	13.8	16.6	18.2	26.8	30.7	31.8
Number of LEDs	15	15	7	4	4	7	8	15

29 The LAMS is an asynchronous autonomous system. Both source and detector are turned on
 30 aboard the ship prior to each deployment and the LAMS is continuously taking data while
 31 lowered and recovered. The only parameters controlled from the ship are depth and time. The
 32 LAMS is connected with the ship only via the deploying steel wire.

33 The light source was constructed using eight groups of industrial LEDs. The manufacturer and
 34 part number of the various LEDs used are given in Reference [10]. The LEDs are not
 35 monochromatic light sources but emit over a significant spectral region. The spectral distributions

1 of the light sources used are shown in Figure 2. They were measured in the laboratory using the
2 LED system mounted inside its glass sphere with a commercial diffraction grating
3 spectrophotometer [11], located outside the glass sphere. The wavelengths λ_m for the peak of the
4 light intensity distributions, the Full Width Half Maximum (FWHM) of the spectra and the
5 number of LEDs used for each wavelength group are given in Table II.

6 A different number of LEDs was used for each wavelength in order to provide adequate light
7 intensity. The LEDs are mounted on a circuit board arranged inside their glass sphere and are
8 located almost in a circular pattern, within a circle of a radius of 3 cm, as seen in Fig.3. Over the
9 small angular region subtended by the light detector of the system, a maximum of $\Delta\phi = \pm 0.15^\circ$
10 for the shortest optical path used, the intensity is uniform in ϕ and therefore, in the absence of
11 absorption, it varies as a function of distance, proportionately to $1/R^2$. This absence of angular
12 dependence was determined by measurements in the laboratory, in air [12], where the opening
13 cone of the each LED assembly was found to have a rough bell shape with FWHM greater than
14 20° in air, or 15° in water, and no significant intensity variation was found over an angular range
15 that matched any possible misalignment, i.e. $\Delta I < 0.5\%$ for $\Delta\theta \approx 2^\circ$ ($\theta = 0^\circ$ defines the direction
16 from the LED source to the centre of light detector).

17 Each LED group is activated sequentially and is controlled by a microcontroller with a crystal
18 oscillator clock to count time. During a measurement cycle the LEDs of a particular wavelength
19 are turned on for 10 seconds, then switched off and after 2 seconds the LEDs of the next
20 wavelength are turned on. Between light cycles a 14 second no-light gap is inserted, and the
21 overall measurement cycle has a period of 110 seconds. The LEDs are driven from a regulated
22 5V source.

23 The light detector consists of two plane photodiodes [13] with a sensitive area of $18 \text{ mm} \times 18 \text{ mm}$
24 and of very uniform spatial response. The photodiode arrangement in the glass sphere is shown in
25 Fig. 4 together with their spectral response as provided by the manufacturer. They are used to
26 form two independent but identical detectors, running on two different data acquisition channels
27 working with a common clock. In each channel, the current, which is proportional to the light
28 intensity on the detector, is converted to voltage, digitised by a 16 bit ADC. The photodiode
29 current is read 75 times each second. It should be noted that this period, also controlled by a
30 crystal oscillator, is not synchronised with the light source cycling. A 512 MB SD memory card is
31 used for data storage. Data is read out of this memory and transferred to a laptop PC using a high
32 speed USB port.

33 Power is supplied by a bank of batteries inside each sphere that houses the source or the detector.
34 The system can operate in a stable autonomous fashion for more than 48 hours on a single set of
35 batteries. The glass spheres are equipped with a vacuum port and a 7-pin water-tight electrical
36 receptacle through which the system is controlled (start/stop and on/off for both the source and
37 the detector units, and data read-out for the detector unit).

38 A typical complete cycle of the system is shown in Fig. 5, where the photodiode response is given
39 in ADC counts. Since all our results are derived from fitting our data to equation 1 an absolute
40 normalization of the light intensity is not required.

41 To reduce the noise the response is heavily damped in the electronics. This explains the long RC
42 time constant in the rising and falling edges. In each light-on measuring period of 10 seconds
43 there are some 750 measurements of the intensity; to avoid complications due to the RC time
44 constant of the detector electronic circuit, we only utilize the data of the last 2/3 of each

1 measuring period, i.e. we use the last 495 samples. Some light sources display a time dependence
2 of their intensity which decreases as a function of time; such variations were taken into account
3 by fitting a straight line to the data of each measuring period. The value of the fit at the latest time
4 of each measuring period gave the corresponding light intensity. We note that this time
5 dependence of the intensity is characteristic for each LED assembly at a given wavelength and
6 does not depend on the length of the optical light path. Therefore it does not affect the intensity fit
7 to the different optical paths, provided the same data analysis procedure is followed. The intensity
8 thus derived was averaged over many cycles (10 to 20 complete 110 second cycles were taken at
9 each depth and wavelength) and as a result the statistical error on the light intensity is very small.
10 A small zero offset, determined by the residual dark current measurements during the no-light
11 gap was subtracted.

12 Another feature of the intensity graphs, Fig. 5, is the presence of occasional small downwards
13 transients. The time structure of these transients indicates that they are due to small decreases of
14 the light intensity reaching the detector. We attribute these to small flakes of particulate matter
15 floating in the field of view of our light sensor. We found that removing those transients does not
16 alter the value of the reported light intensity of each measuring period. Such transients were seen
17 in all of the deployments and are consistent with the frequency and size of observed larger
18 particulate matter seen in video surveys of the deep sea [14].

19

20 3. Measurement details and data analysis

21 In a neutrino underwater telescope, such as the proposed KM3NeT, the light detecting optical
22 modules are sparsely deployed in the deep sea and thus, as already mentioned, we are in the
23 situation of an open geometry where there is no collimation of the detected light. Therefore the
24 use of an uncollimated beam, such as the one of the LAMS, is appropriate for a measurement of
25 the transmission of light over different lengths of water paths. The light intensities of the LED
26 sources as detected by the photodiode, $I(\lambda, R)$, at various but fixed distances (light paths) R
27 between the source and the detector are recorded and compared to each other. As a result we do
28 not need any external or absolute calibration.

29 Laboratory tests of the LAMS in air show that the attenuation of light intensity is almost totally
30 due to a geometrical spreading of the beam and follows with high accuracy the $1/R^2$ law. The
31 LAMS was tested in air before and after each deployment and its characteristics remained the
32 same. Given the fact that the attenuation length in air for a clear standard atmosphere is 4 to 7 km
33 for the visible light range [15], our instrument is not of sufficient length to reliably measure it.

34 The intensity data are divided in data sets. Each set combines all the data for a particular depth for
35 each stationary deployment, for each specific LAMS length, and for each LED source (i.e.
36 wavelength range). The light intensity measurements were combined and averaged and as a result
37 instrumental noise is highly suppressed. We use this mean intensity $I(\lambda, R)$ and its statistical error
38 for further analysis. We have added in quadrature an additional 0.5% error in the intensity as an
39 estimate of systematic uncertainties of the angular dependence as described in section 2.1. Then,
40 for each set, the intensity data for each wavelength range are fit to equation (1). We have allowed
41 for a ΔR variation in the arm lengths of $\Delta R = \pm 2$ cm for 10.00 m arm length, $\Delta R = \pm 3$ cm for
42 15.10 m, $\Delta R = \pm 3$ cm for 17.17m, and $\Delta R = \pm 4$ cm for 22.27 m, in the fit to account for any
43 uncertainty in the light path and for the thickness of the curved envelopes of the glass spheres.
44 From the fit we determine I_0 (which we use as a check of the stability of the source) and the

1 transmission length L_β and its error for each wavelength. The data follow the combined $1/R^2$ and
2 the Beer-Lambert Law very well; a typical example of a fit is shown in Fig. 6.

3 The system was suspended from a 12 mm diameter steel wire cable and was lowered into the sea,
4 at a speed of less than 1 m/s, from the deployment vessel. The depth where the LAMS was
5 located was calculated from the length of the deployed steel wire using the ship's wire length
6 measuring device[†]. The measured length using this device was compared with the depth
7 determined from a pressure sensor attached on the LAMS and the difference was less than 10
8 meters. The duration of the measurement at each station was about 20 minutes, while at the
9 deepest stations the measurement duration was about 40 minutes. After each recovery, the length
10 of the LAMS light path was changed on deck by adding girder sections, as described above, while
11 the data were recovered from the LAMS memory.

12 **4. Results**

13 Tables III - VI show the transmission length measurements for all deployments where the LAMS
14 was stationary. Since the LAMS keeps taking data throughout its descent and ascent we have
15 collected data at all depths while the instrument was moving. We are not presenting at this time
16 results from the descending and ascending periods; the analysis of these data is ongoing and will
17 provide a more detailed profile of the light transmission as a function of sea depth. Tables VII and
18 VIII show the ratios of the transmission lengths at the sites measured in May 2009 for the depths
19 around 3000 m and also at the deepest depths, where the neutrino telescope elements will be
20 located. Fig. 7 shows the transmission length measurements from the Pylos sites.

21 The data are presented as being taken at the peak of the spectral distribution of each light source.
22 We have not taken into account the spectral shape of the various LED sources, nor have we
23 integrated over the spectral response of the photodiode.

24 **5. Discussion**

25 We will focus on three aspects of the variation seen in our measurements of the transmission
26 length:

- 27 • depth dependence, where the transparency changes with depth,
- 28 • temporal effects, i.e. the transparency depends on the season, and
- 29 • site dependence, i.e. the variation in the transmission length for different sites
30 but at similar depths but only for measurements taken within a few days of each
31 other.

32 **5.1 Depth dependence of the transmission:**

33 The variation of the transmission length for various depths is about 2 to 5 m with shorter
34 transmission lengths for shallower waters and is about the same at all sites. The transmission
35 length always reaches a maximum at depths 3000m – 3400m. These data are consistent with the
36 results of previous measurements at three different nearby sites[16], performed with an early
37 version of a similar system, albeit our measurements always lie at the lower limit of the
38 uncertainty of the earlier data, as shown in Fig. 8.

[†] A pulley with a turn-counting unit

1 The measurements reported here correlate well with the data of Ref. [2], where the depth-
 2 dependence of hydrological and optical parameters are explained by the presence of waters of
 3 different origin at different depths: at ~3300 m there is water that originates in the Cretan Sea and
 4 thus is characterised by higher salinity, temperature and optical transparency; at depths below
 5 ~3600 m, there is water of Adriatic origin as is indicated by the decreasing salinity and water
 6 transparency. This Adriatic water is newly formed, i.e. it was recently at the surface and has been
 7 sub-ducted at those depths due to dense water formation during some recent winter season. At
 8 depths greater than ~5000 m the oxygen values are decreasing and this is indicative of some
 9 isolated old Adriatic water mass that is found in the bottom layers of the N5.2D site.

Table III:

Transmission Length, L_{β} , in metres at site N4.5D, April 2008 deployments. The reader should note that different light sources with slightly different wavelength are used in April 2008 compared to those used in the subsequent deployments.

Depth (m)	Date	λ (nm)							
		374.8	379.8	402.2	424.2	445.6	461.2	504.0	519.1
2500	Apr.08	20.8±0.2	25.6±0.3	31.3±0.8	42.2±0.8	41.7±0.8	42.9±1.5	27.9±0.4	22.5±0.3
3400	Apr.08	20.8±0.2	24.9±0.3	31.1±0.8	42.8±0.9	42.6±0.9	45.7±1.7	28.1±0.4	22.3±0.3
4100	Apr.08	20.6±0.2	22.5±0.3	28.0±0.7	41.4±0.8	41.5±0.8	40.1±1.3	27.7±0.4	21.1±0.2

10

Table IV:

Transmission Length, L_{β} , in metres at site N5.2D, October 2008 deployments

Depth (m)	λ (nm)							
	375.7	385.7	400.3	425.0	445.4	462.6	501.6	519.5
2000	21.5±0.3	25.4±0.3	29.8±0.4	40.3±0.8	42.3±0.8	42.8±0.9	30.2±0.5	21.3±0.2
3000	21.6±0.3	26.0±0.3	30.7±0.5	41.8±0.8	44.7±0.9	45.1±0.9	30.8±0.5	21.6±0.3
4000	20.6±0.2	24.3±0.3	28.5±0.4	38.6±0.7	40.9±0.8	41.7±0.8	29.4±0.4	20.9±0.2
4900	20.3±0.2	24.1±0.3	28.3±0.4	38.0±0.7	40.4±0.8	40.6±0.8	29.3±0.4	20.6±0.2

11

Table V:

Transmission Length, L_{β} , in metres at site N4.5D, October 2008 and May 2009 deployments

Depth (m)	Date	λ (nm)							
		375.7	385.7	400.3	425.0	445.4	462.6	501.6	519.5
2000	Oct.08	21.2±0.2	25.4±0.3	29.3±0.4	40.4±0.8	40.5±0.8	42.2±0.8	29.8±0.4	21.0±0.2
	May 09	20.8±0.5	24.0±0.7	28.4±0.8	34.7±1.2	39.4±1.6	42.0±1.7	27.8±0.8	20.9±0.5
2500	Oct.08	21.6±0.3	26.1±0.4	30.5±0.5	42.7±0.9	42.5±0.9	44.6±0.9	30.6±0.5	21.4±0.2
	May09	21.7±0.5	25.4±0.6	30.0±0.9	36.3±1.3	41.9±1.7	45.5±2.0	28.6±0.8	21.4±0.5
3000	May09	21.9±0.5	25.7±0.7	30.5±1.0	37.8±1.5	43.8±1.9	47.2±2.2	29.3±0.9	21.5±0.6
3400	Oct.08	21.4±0.2	25.9±0.3	30.1±0.5	43.0±0.9	42.2±0.8	43.8±0.9	30.4±0.5	21.5±0.2
	May09	21.9±0.5	25.7±0.7	30.4±1.0	38.2±1.4	44.3±1.9	47.8±2.2	29.8±0.9	21.9±0.6
4100	Oct.08	20.5±0.2	24.7±0.3	28.4±0.4	39.7±0.8	39.8±0.8	41.5±0.8	28.0±0.4	20.9±0.2
	May09	21.0±0.5	24.8±0.7	29.2±0.9	36.0±1.3	42.3±1.8	46.1±2.0	28.7±0.8	21.3±0.5

12

Table VI:*Transmission Length, L_{β} , in metres at sites CP1 and CP2, May 2009 deployments*

Depth (m)	Site	λ (nm)							
		375.7	385.7	400.3	425.0	445.4	462.6	501.6	519.5
2000	CP1	19.6±0.4	22.9±0.6	27.1±0.7	32.6±1.1	37.8±1.4	39.4±1.6	26.7±0.8	20.8±0.5
	CP2	17.6±0.4	20.4±0.5	23.8±0.6	28.6±0.8	33.1±1.2	35.8±1.3	24.9±0.7	19.4±0.4
2500	CP1	20.1±0.5	23.6±0.6	28.1±0.8	34.5±1.2	40.2±1.6	42.4±1.8	27.9±0.8	21.4±0.5
	CP2	18.2±0.4	21.2±0.5	24.8±0.7	30.4±0.9	34.9±1.3	38.0±1.4	25.8±0.7	19.9±0.4
3100	CP1	19.9±0.4	23.2±0.6	27.8±0.8	34.6±1.2	41.5±1.7	44.1±1.9	28.5±0.8	21.8±0.5
3000	CP2	19.5±0.4	23.0±0.5	27.3±0.8	34.1±1.2	39.6±1.6	43.7±1.8	27.6±0.8	21.1±0.5
3400	CP2	18.6±0.4	21.8±0.5	25.6±0.7	32.4±1.1	38.5±1.5	42.0±1.7	27.1±0.8	20.9±0.5

1

Table VII:*Comparison (ratios of transmission lengths) at the three sites measured in May 2009, for similar depths (i.e. 3000-3100 m)*

Ratio	λ (nm)							
	375.7	385.7	400.3	425.0	445.4	462.6	501.6	519.5
N4.5D (3000m) ÷ CP1 (3100m)	1.10 ± 0.03	1.11 ± 0.04	1.10 ± 0.05	1.09 ± 0.06	1.06 ± 0.06	1.07 ± 0.07	1.03 ± 0.04	0.99 ± 0.04
N4.5D (3000m) ÷ CP2 (3000m)	1.12 ± 0.03	1.12 ± 0.04	1.12 ± 0.05	1.11 ± 0.06	1.11 ± 0.07	1.08 ± 0.07	1.06 ± 0.04	1.02 ± 0.04

2

Table VIII:*Comparison (ratios of transmission lengths) at the three sites measured in May 2009, for the maximum deployment depths at each site.*

Ratio	λ (nm)							
	375.7	385.7	400.3	425.0	445.4	462.6	501.6	519.5
N4.5D (4100m) ÷ CP1 (3100m)	1.06 ± 0.03	1.07 ± 0.04	1.05 ± 0.04	1.04 ± 0.05	1.02 ± 0.06	1.05 ± 0.06	1.01 ± 0.04	0.98 ± 0.03
N4.5D (4100m) ÷ CP2 (3400m)	1.13 ± 0.04	1.14 ± 0.04	1.14 ± 0.05	1.11 ± 0.06	1.10 ± 0.06	1.10 ± 0.07	1.06 ± 0.04	1.02 ± 0.03

3

5.2 Temporal effects

4 In fig. 9 we show the temporal variability of the water transparency at the Pylos site. The data of
 5 April 2008 and October 2008 are consistent with each other, however both of these spectra differ
 6 from the one of May 2009, mainly for the wavelengths 425.0 and 462.9 nm (see Fig.7). We
 7 cannot show any temporal variability at Capo Passero site since data were taken with the LAMS
 8 only in May 2009; however in [18] it is reported that at the of Capo Passero there are
 9 considerable time variations in absorption spectra of deep water for the wavelengths 412 nm and
 10 440 nm.

12 It is well known from oceanographic studies that variations of the optical parameters of sea water
 13 depend on the wavelength and are caused by changes in the water's composition. As noted in [7],
 14 in the wavelength range of 390 – 470 nm the contribution to scattering from submersed particles

1 dominates, while dissolved organic materials (the so-called ‘yellow substance’) account for 83 to
2 95% of the light attenuation in sea water. Thus, the variability of the transmission length of deep
3 water is almost completely caused by changes in concentration of submersed particles and of the
4 ‘yellow substance’. Temporal variations of the water optical parameters at the Pylos and the Capo
5 Passero areas can be explained as being the result of underwater processes when water masses
6 stratify due to density differences but also undergo some vertical migration through dynamic
7 circulation structures (cyclones or anticyclones) present in the Eastern Mediterranean [17].

8 **5.3 Site dependence**

9 Even though the transmission length differences between the N4.5D and the N5.2D sites are
10 small (about one meter as seen in Fig. 7b and Fig. 7c), the transmission length at Capo Passero is
11 about 10% shorter than the transmission length at the Pylos site. However, the spectral shapes of
12 the transmission length at all sites are very similar, as shown in Fig. 10.

13 **5.4 Comparison of transmission and attenuation spectra**

14 A comparison of the transmission length spectrum with the spectrum of the attenuation length
15 measured with a transmissometer configuration using a highly collimated beam [19] (see Fig. 11a)
16 shows that the transmission length exceeds the attenuation length at wavelength $\lambda < 490$ nm,
17 but at $\lambda > 490$ nm transition length coincides with attenuation length of pure sea water. This
18 feature can be explained by the characteristics of light scattering and absorption by sea water. It is
19 known that for long-wavelengths, scattering is very weak and in that region of the spectrum the
20 attenuation is mainly due to the absorption of photons by water molecules [7]. The presence of
21 dissolved impurities and suspended particles does not have any effect. However, with decreasing
22 wavelength the scattering increases, and in the violet region close to the UV the absorption of
23 photons by molecules of dissolved organic material (‘yellow substance’) begins to dominate
24 while absorption by water molecules has become negligible.

25 **6. Conclusions**

26 The transparency of deep sea water has been measured with the LAMS (Long Arm Marine
27 Spectrophotometer) in two well separated sites in the Western and Eastern Ionian Sea in order to
28 study optical parameters at locations where the KM3NeT large underwater neutrino telescope
29 may be deployed. An uncollimated light source of eight different wavelength ranges was used to
30 measure the optical parameters in the spectral region where the optical detection units of the
31 neutrino telescope (bi-alkali photocathode photomultipliers) have quantum efficiency larger than
32 a few percent.

33 The values of the transmission length measured in the Eastern Ionian Sea (Pylos N4.5D and
34 N5.2D sites) are in good agreement with each other and with earlier measurements. Light
35 transmission lengths in the Eastern Ionian are 10% longer than the ones measured in the Western
36 Ionian. The optical properties at the Pylos site have a weak depth dependence but are laterally
37 homogeneous over a large geographic region (~ 1000 km²), and although there are $\sim 15\%$ seasonal
38 variations for violet-blue wavelengths the transmission lengths are compatible with being
39 constant over the investigated multiyear timescale, 1994 to 2009.

40 In a broad wavelength range the transmission length coincides systematically with the attenuation
41 length, while in the region between, roughly, 420-480nm it exceeds it. The large difference
42 between the two, at around 510nm, is probably due to the very steep slope of both attenuation and
43 transmission length, combined with small uncertainty in the wavelengths of the different light
44 sources used in 1992 and 2009.

1

2 **7. Acknowledgements and dedication**

3 We thank our electronics and machine shop teams and our colleagues from the Hellenic Centre
4 for Marine Research for their help, especially the former Director George Chronis as well the
5 Captain, Officers and Crew of the R/V “Aegaeo”. We also thank our colleagues John Learned of
6 the University of Hawaii and Hank Crawford of the University of California, Berkeley, for their
7 overall help and for many helpful discussions throughout many years.

8 Parts of this Research have been funded by a Centre of Excellence award of the General
9 Secretariat for Research and Technology of the Ministry of Development of Greece, and by the
10 EU in the 6th Framework Program under Contract Number 011937. We also thank the
11 Hamamatsu Photonics Co for providing the photodiodes gratis.

12 We dedicate this paper to the memory of our good friend, mentor, and collaborator, Hugh
13 Bradner, Professor of Engineering Physics and Geophysics, Institute of Geophysics and Planetary
14 Physics, Scripps Institution of Oceanography, University of California, San Diego and former
15 Associate Director for Particle Physics, Lawrence Radiation Laboratory.

16

17 **References:**

18 [1] A. Achterberg *et al.*, “*First Year Performance of the IceCube Neutrino Telescope*”,
19 *Astroparticle Physics* **26**, (2006), 155-173. Website: <http://icecube.wisc.edu>

20 [2] KM3NeT Conceptual Design Report, April 2008, 118 p., ISBN 978-90-6488-031-5.
21 Website: <http://www.km3net.org/>

22 [3] L. K. Resvanis for the NESTOR coll., “*NESTOR: A Neutrino Particle Astrophysics*
23 *Underwater Laboratory for the Mediterranean*”, in Proceedings of the High Energy Neutrino
24 Astrophysics Workshop; V. J. Stenger, J. G. Learned, S. Paksava and X. Tata editors Hawaii,
25 325, (1992), World Scientific, Singapore, Website <http://www.nestor.noa.gr>, and

26 G. Aggouras *et al.*, “*A measurement of the cosmic-ray muon flux with a module of the*
27 *NESTOR neutrino telescope*”, *Astroparticle Physics* **23**, 377-392, 2005, and

28 G. Aggouras *et al.*; “*Operation and performance of the NESTOR test detector*”, *Nucl.Instr. &*
29 *Methods in Phys. Res. Sect. A*, 2005, Vol.: 552, Issue: 3, pp. 420-439

30 [4] E. Migneco *et al.*, “*The NEMO Project*”, Proceedings of the VLvNt Workshop pp 5-10,
31 NIKHEF, Amsterdam, 5-8 October 2003. Website <http://nemoweb.lns.infn.it>

32 [5] N. G. Jerlov, “*Optical Oceanography*”, American Elsevier, New York, 1968.

33 A.S. Monin. *Ocean Optics; Physical Optics of the Ocean*. Chapter 7, Paragraph
34 7.1,(Scattering properties of sea water) p.167-179.(In Russian)

- 1
2 M.Jonasz and G.R.Fournie. Light Scattering by Particles in Water. Theoretical and
3 Experimental Foundations. 2007 Elsevier Inc., Chapter 4. Paragraph 4.4.2.1,(Scattering
4 coefficients)p.210-216.
- 5 [6] H. Bradner and G. Blackinton, Appl. Opt. 23 (1984) 1009, and
6
7 H. Bradner *et al.*, “Attenuation of Light in Clear Deep Ocean Water”, in Proceedings of the
8 2nd NESTOR International Workshop, October19-21, 1992 , Pylos, Greece, ed. by L. K.
9 Resvanis (1992), p. 247.
- 10
11 [7] A. S. Monin (editor), “Ocean Optics; Physical Optics of the Ocean”, Nauka, Moscow, 1983,
12 pp. 225, 226, and 234 (in Russian).
- 13 [8] R. Smith and K. Baker, “Optical properties of the clearest natural waters (200 – 800 nm)”,
14 Applied Optics **20**, 177, (1981), derived from table I.
- 15 [9] Made of a borosilicate glass (Pyrex), by Teledyne Benthos Inc., North Falmouth, MA, USA
- 16 [10] “375 nm” NSHU590A, Nichia Corp., Tokushima, Japan ; “385 nm” LED385, Roithner
17 Lasertechik GmbH, Vienna, Austria; “400 nm” LED3-UV-400-30, Bivar Inc., Irvine, Calif.,
18 USA, ; “425 nm” LED425-6-3U, Roithner Lasertechik GmbH; “450 nm” LED450-01U,
19 Roithner Lasertechik GmbH; “470 nm” L-7104QBC-D Kingbright Elec. Co., Taipei, Taiwan;
20 “495 nm” NSPE510S Nichia Corp. ; “525 nm” NSPG510S Nichia Corp.
- 21 [11] Model USB4000 Spectrophotometer, manufactured by Ocean Optics Inc., Dunedin, Florida,
22 USA. As used the USB4000 was equipped with a 25 μm slit and a UV grating (Grating type H1,
23 1600 grooves/mm, useful range 200 to 575 nm, peak sensitivity 300 nm) and had an intrinsic
24 FWHM resolution of 1.3 nm. The data of fig. 2 have not been corrected for the spectral
25 dependence of the response of the USB4000.
- 26 [12] S. Koutsoukos *et al.*, NESTOR-Note-010.2009 (unpublished), and
27 E. Chaniotakis, A.Hadjitheodorou, and G.Karathanasis, NESTOR-Note-075.2009
28 (unpublished).
- 29 [13] Large Area Si Photodiode Part no. S6337-01, Hamamatsu Photonics K. K., Hamamatsu,
30 Japan
- 31 [14] I.G. Priede, private communication, based on the deployment of an ISIT camera in the
32 Ionian Sea. The technique is described in A. J. Jamieson *et al.*, “Illumination of trawl gear by
33 mechanically stimulated bioluminescence”, Fisheries Research **81**: 276 (2006).
- 34 [15] See Table 7.4 in S. L. Valley (editor), “Handbook of geophysics and space environments”,
35 Air Force Cambridge Research Center, Bedford, Mass. USA, and also McGraw-Hill, New York
36 (1965), also presented in Fig. 7-3 of “Electro-Optics Handbook”, R.W. Engstrom (Ed.), RCA
37 Corp., Technical Series EOH-11, Lancaster, Penn. 1974.
- 38 [16] E.G. Anassontzis *et al.*, “Light transmissivity in the NESTOR site”, Nuclear Instruments and
39 Methods **A349**, 242-246, (1994).

- 1 [17] H. Kontoyiannis *et al.*, “*Water-Mass Structure and Deep Currents in the NESTOR Area*”,
2 2009, 7p., Contribution to the KM3NeT Design Study, Work Package 5 (unpublished).
- 3 [18] G. Riccobene *et al.*, “*Deep sea water inherent optical properties in The Southern Ionian*
4 *Sea*”, *Astroparticle Physics* **27** (2007) 1-9.
- 5 [19] S. A. Khanaev *et al.*, “*Measurements of water transparency South-West of Greece*”, in
6 *Proceedings of the 2nd NESTOR International Workshop, October 19-21, 1992, Pylos, Greece*,
7 ed. by L. K. Resvanis (1992), p. 253.

8

ACCEPTED MANUSCRIPT

1 WATER TRANSPARENCY MEASUREMENTS IN THE DEEP IONIAN SEA

2 *Captions*

3 **Fig. 1:** LAMS –The Long Arm Marine Spectrophotometer. **Left:** Schematic of the apparatus;
4 **Right:** LAMS ready for deployment on the deck of the R/V “Aegaeo”.

5 **Fig. 2:** LED light source spectra (normalised to same max intensity) measured by the
6 spectrophotometer.

7 **Fig. 3:** Light source; cluster of LEDs inside a glass sphere (left), and close-up of the same
8 (right).

9 **Fig. 4:** Light detector system; the two Si large area Hamamatsu S6337-01 Si photodiodes (left)
10 and their spectral response [13] (right).

11 **Fig. 5:** Typical cycle of raw data obtained by the LAMS, at the N45 site at 4100m deep in
12 October 2008. This data is from a configuration with optical path of 10m and shows that even in
13 this case, where the light intensities are highest, the ADC is not saturated.

14 **Fig. 6:** Typical result of the fit. The data are points with error bars (not visible because they are
15 too small), and the line is the fit to eq. (1).

16 **Fig. 7.** Data obtained in the Pylos N4.5D and N5.2D sites (if an error bar is not shown, then it is
17 smaller than the symbol size).

18 **a:** April 2008, N4.5D site;
19 **b:** October 2008. N4.5D site;
20 **c:** October 2008, N5.2D site;
21 **d:** May 2009. N4.5D site.

22 **Fig. 8.** Data obtained at the Pylos N4.5D site. Comparison of the LAMS data at 460- 470 nm
23 wavelength (October 2008, with results from 1994 for three different nearby sites[16]). (If an
24 error bar is not shown, then it is smaller than the symbol size).

25 **Fig. 9.** Transmission length measured in April 2008, October 2008, and May2009 at the Pylos
26 N4.5D site; depth 4100 m (if an error bar is not shown, then it is smaller than the symbol size).

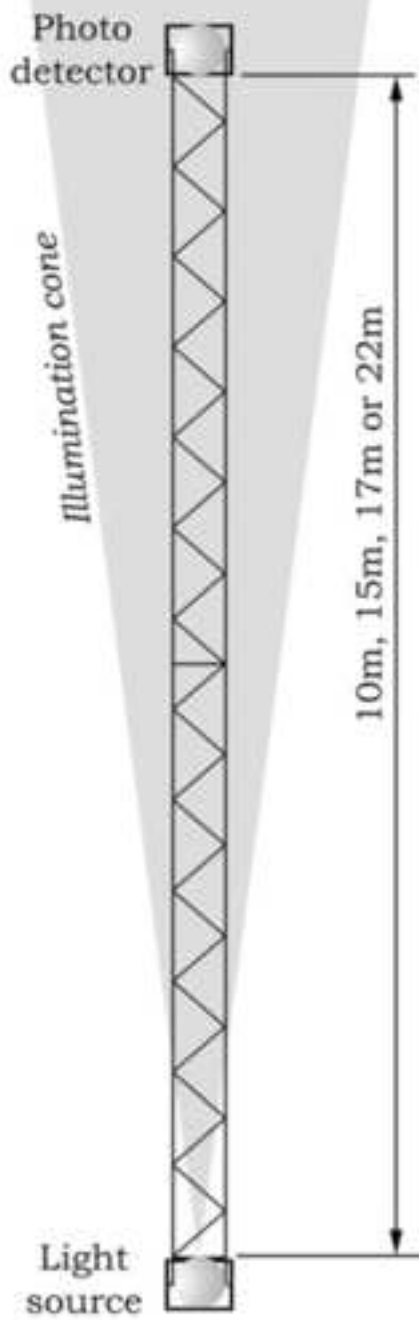
27 **Fig. 10.** Transmission length versus wavelength at the Capo Passero and Pylos sites (if an error
28 bar is not shown, then it is smaller than the symbol size).
29 **a:** for similar depths; **b:** for the maximum deployment depths (at about 300 m above seabed).

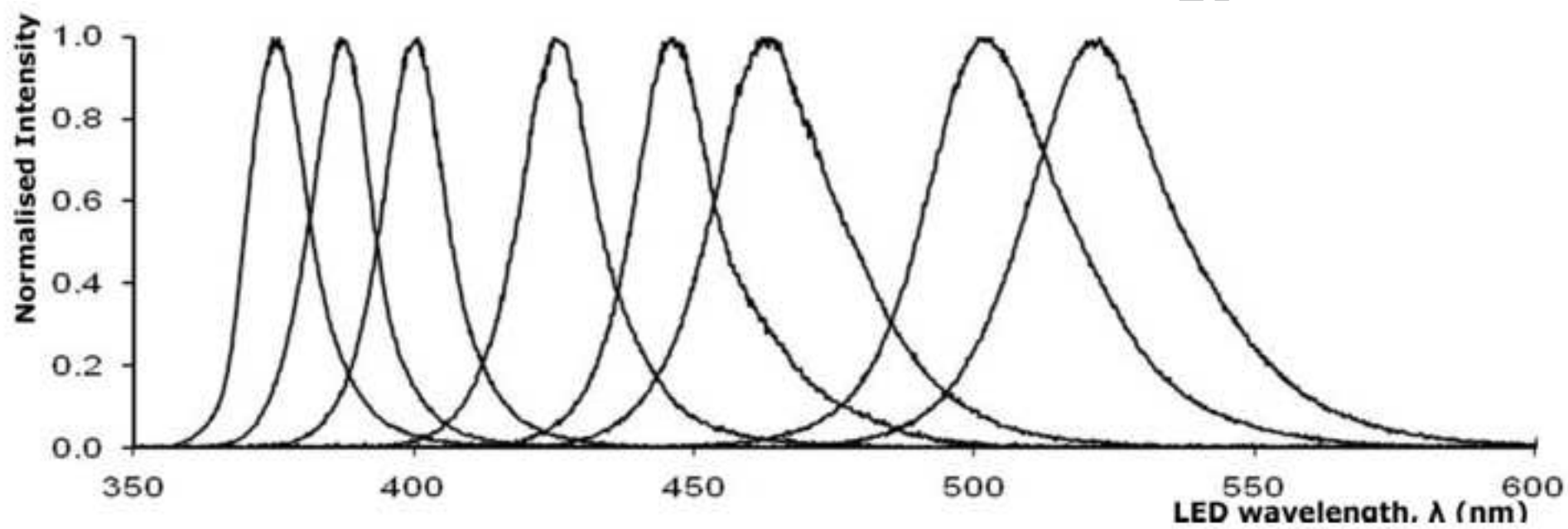
30 **Fig. 11.** Transmission or attenuation lengths at the Pylos and Capo Passero sites.

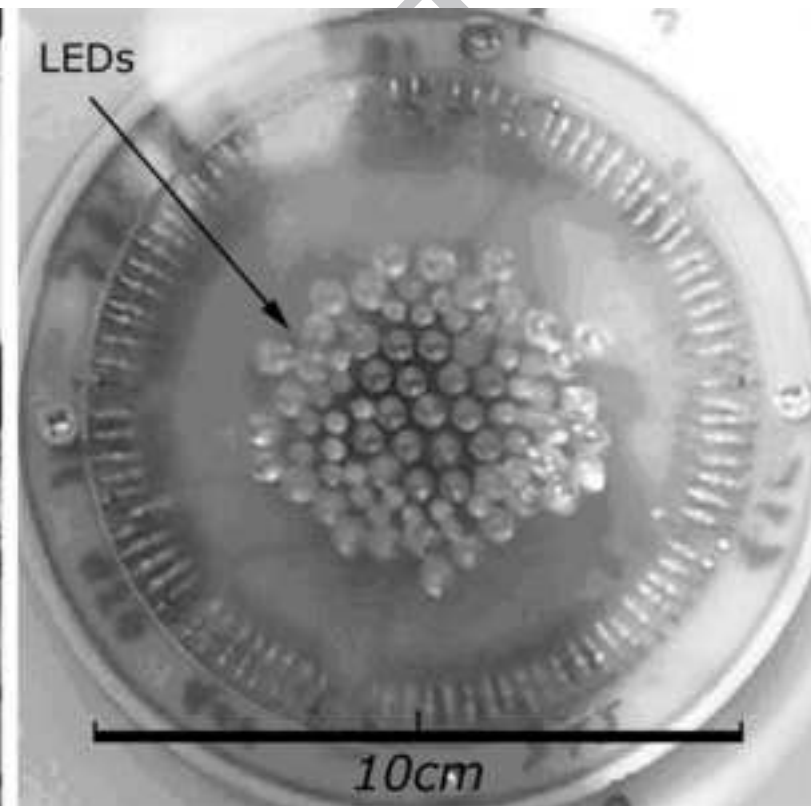
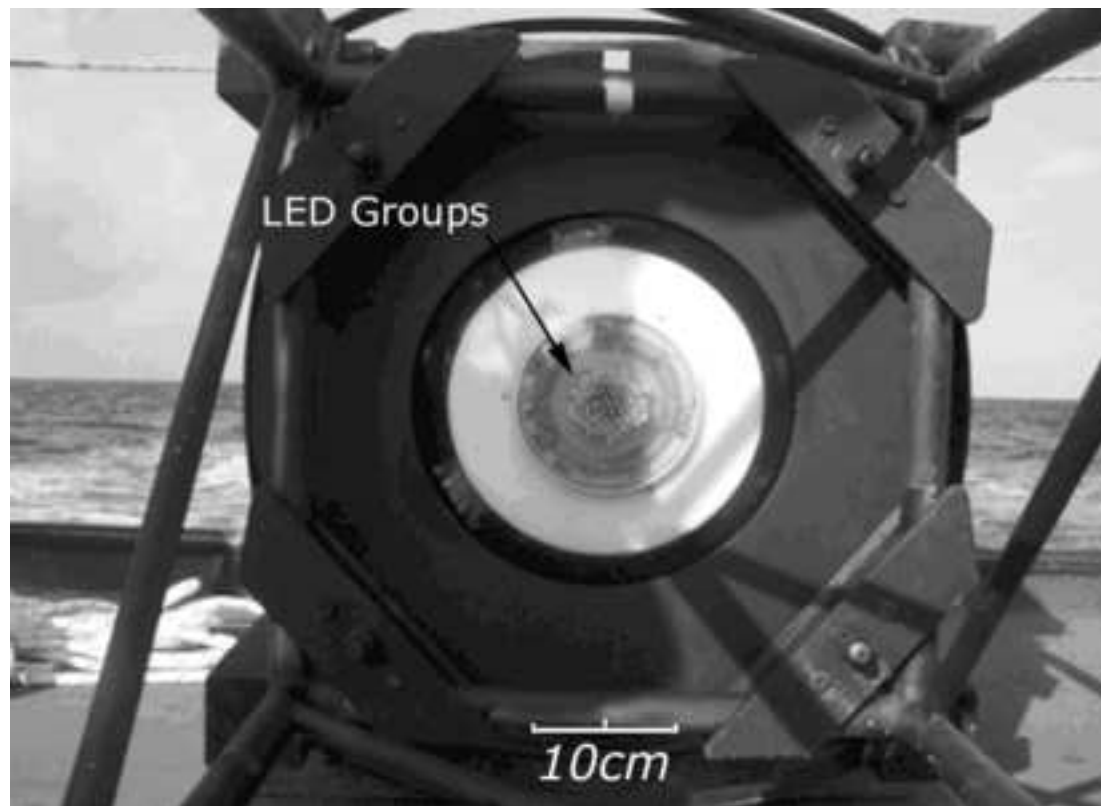
31 **a:** Transmission lengths: at N4.5D site at 3400 m, May 2009 (triangles); Attenuation lengths at
32 depth 3800 m, Oct. 1992 (squares [19]).
33 **b:** CP1 site, Transmission lengths at 3100 m, May 2009 (triangles); attenuation lengths at 2850
34 – 3250 m from [18], Dec.1999 (open circles), March 2002 (open crosses), May 2002 (open
35 squares), August 2002 (open triangles) and July 2003 (open diamonds). The attenuation lengths
36 for pure sea water are from [8].

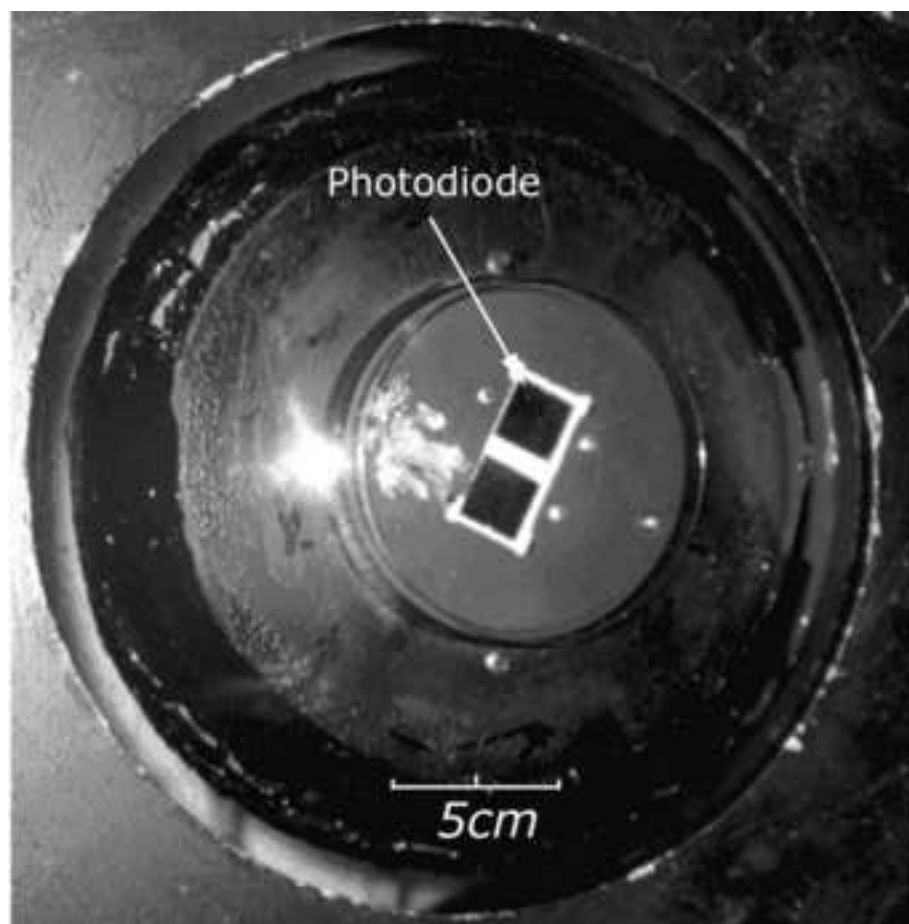
37

Figure1









■ Spectral response

